DOI: 10.1111/cgf.14106
ACM SIGGRAPH / Eurographics Symposium on Computer Animation 2020
J. Bender and T. Popa
(Guest Editors)

Volume 39 (2020), Number 8

Distant Collision Response in Rigid Body Simulations

E. Coevoet[1] and S. Andrews[2]and D. Relles[1] and P.G. Kry[1]

[1]McGill University, Canada
[2]École de technologie supérieure, Canada

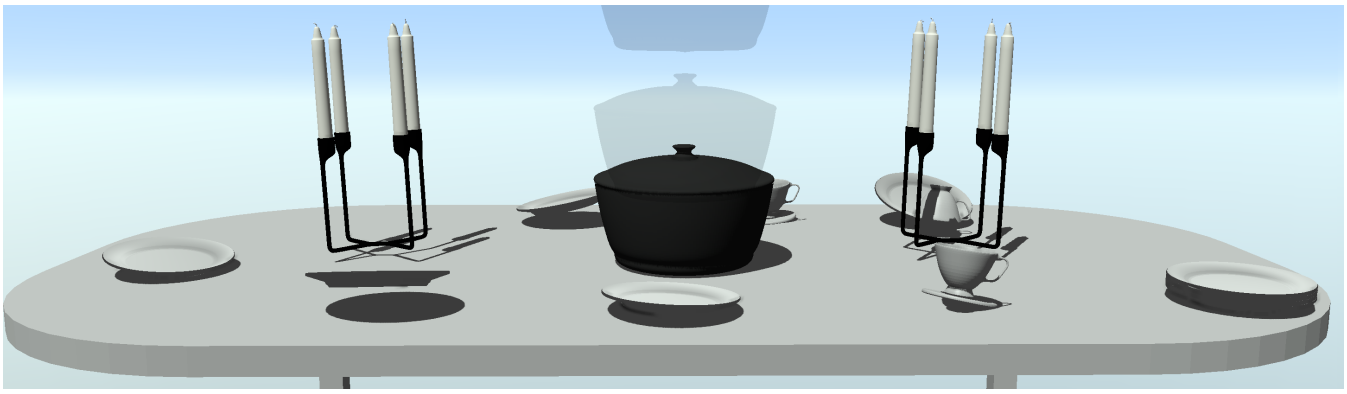

Figure 1: *Dinner is served! A large pot dropped on a table causes plates and cups to jump. While all objects are rigid bodies, we approximate the elastic vibrations and shock waves due to large force changes in order to produce a distant collision response.*

Abstract

We use a finite element model to predict the vibration response of objects in a rigid body simulation, such that rigid objects are augmented to provide a plausible elastic collision response between distant objects due to vibration. We start with a generalized eigenvalue decomposition of the elastic model to precompute a response to an impact at any point on an elastic object with fixed boundary conditions. Then, given a collision between objects, we generate an approximate response impulse to distribute to other objects already in contact with the colliding bodies. This can lead to distant impacts causing an object to slip, or a delicate stack of objects to fall. We also use a geodesic distance based spatial attenuation approximation for travelling waves in objects to respond to an impact at one contact with an impulse at other locations. This response ultimately allows a long distance relationship between contacts, both across a single object being struck, but also traversing the contact graph of a larger collection of objects. We qualitatively validate our approach with a ground truth simulation, and demonstrate a number of scenarios where a long distance relationship between contacts is valuable.

CCS Concepts

•***Computing methodologies*** → *Collision detection;* ***Animation;***

1. Introduction

Rigid body simulations are an integral component of many interactive and real-time computer graphics applications. However, when contact is involved, rigid body simulations do not capture the true behavior of a response due to impact, such as transient vibration effects. These effects can be observed in everyday scenarios, for instance, when a heavy object is dropped on a table and other nearby objects resting on the table will momentarily rattle (see Figure 1). These disturbances are due to waves that emanate from the site of an impact on an elastic object, and produce small vibrations across the object's interior and surface.

It is common to ignore the elastic properties of rigid bodies in most simulations, with one exception: the use of a coefficient of restitution to approximate how objects should bounce off one another. While the true response to collision can vary widely based on the impact location, the one parameter Newton restitution model

is widely used and does a very reasonable job of capturing the basic phenomenon. With the goal of producing visually richer rigid body simulations, bounce maps [WSJP17] provide collision-location specific restitution coefficients, but only focus on the local effect. Our goal is similar, except that we focus on the subtle relationship between an impact at one location and distant contacts at other locations.

If we treat a rigid body as a stiff elastic solid, we can use a finite element model simulation with small step sizes to create a faithful approximation for how collision will produce a response at distant existing contacts. The collision produces elastic waves that propagate through the material, reflect at boundaries, and ultimately produce complicated vibrations. Such simulations require very small time steps to properly capture wave propagation in stiff materials. So, to avoid this high computational cost, we propose two simple and inexpensive approximations that can be easily incorporated into interactive rigid body simulations stepped at normal rates (e.g., video frame rates). First, we use a reduced modal model to asses the displacements of low frequency vibrations produced by impacts. We use the maximum observed displacement of these vibrations at distant contacts to produce a response. Secondly, we propose a method to simulate the effect of wave propagation in larger objects (for instance, terrain) where attenuation due to distance should be considered. Although the underlying physical effect is the same for small and large objects, we note that reduced modal models are best for smaller objects that resonate when hit, while our spatial attenuation model is better for larger objects in which traveling waves are poorly modeled with a reduced modal basis.

Overall, our primary contribution is an efficient algorithm for simulating the distant transient effects due to impacts in real-time rigid-body simulations. Our method is straightforward and can account for vibrations in small objects, and traveling waves in terrain or large objects. We demonstrate the effect of a distant collision response in a number of practical applications, and provide a comparison with a ground truth elastic simulation using small time steps. Finally, we discuss the limitations of our simplifications to the problem.

2. Related Work

Bender et al. [BET13] provide an excellent survey of rigid body simulation with frictional contact. Included in this survey is a discussion of the single parameter coefficient of restitution models attributed to Newton and Poisson, as well as the multi-parameter model of Chatterjee and Ruina [CR98], which allows frictional effects to be accounted for in the collision response. Cataldo and Sampaio [CS01] provide a short yet informative survey of other rigid body collision models used in mechanical engineering. More recently, Wang et al. [WSJP17] propose storing texture maps of precomputed collisions responses, and a method for combining information stored at the point of impact on each surface to produce a coefficient of restitution specific to the geometry of two colliding objects. While this adds visual richness to a rigid body simulation, we note that this only addresses the local problem. In our work, we use the simple and common Newtonian coefficient of restitution, and instead focus on the impulses that distant contacts should receive when there is an impact elsewhere on the object.

Our approach augments a rigid body simulation to provide a better approximation of how an effectively-rigid body should behave in the real world. In addition to the bounce maps technique for varying the coefficient of restitution [WSJP17], other work has recognized the importance of not overlooking the true elastic properties of rigid bodies, specifically, in the production of contact sounds. FoleyAutomatic [vdDKP01] uses models built from impact recordings of real objects to produce sounds in simulations of rigid bodies in contact, while O'Brien et al. [OSG02] generate impact sounds by first precomputing the vibration modes of finite element models. Zheng and James [ZJ11] propose a method for high quality modal sound simulations where they take all contacts (i.e., changing boundary conditions) into account, and produce coupled motions that would not otherwise be produced in a rigid body simulation. While these simulations feature realistic collision response and high-quality contact sounds, they are only produced with a large computational cost.

In addition to impact responses and sound, augmenting rigid bodies to allow visually rich simulations has been proposed for other physical properties. Just as we can use textures to make the visual appearance of simple geometries more complex, Coulomb friction textures can be measured and reused [PDJ*01], and spatially varying friction properties can be designed with phenomenological models [EMAK20]. Galoppo et al. [GOM*06] propose elastic deformation textures to model the varying surface compliance of *almost* rigid bodies. They treat the body as having a rigid core surrounded by a layer of deformable material, and propose a method for efficient decoupled contact resolution. For the coupled formulation, implicit integration ensures stability but also inhibits the production of any distant impact responses. For the quasi-static case, Pauly et al. [PPG04] propose a Boussinesq approximation to local deformation on rigid bodies. In contrast, our simulations remain rigid as we do not seek to visualize any deformation of the surface due to contact.

We note that the relationship between different contacts is important in several problems related to solving for the motion of rigid bodies in contact. While not directly related to our problem of distant collision response, we note a few examples here. For instance, Smith et al. [SKV*12] resolve the problem of simultaneous reflections during an impact on a rigid body system. Their approach produces the correct response for a Newton's cradle, i.e., when a sphere strikes one end of the row of spheres, an impulse on the sphere at the far end is generated to correctly transfer the momentum. For interactive rigid body simulations using iterative solvers, shock propagation [Erl07] is likewise a useful technique for more quickly converging to a solution due to a distant collision. In other examples that concern improving convergence, long distance constraints for cloth, chains, and gears have been proposed [KCMF12, MCMJ17]. While we must also address the problem of computing solutions to time step rigid body systems with frictional contact, our goal in this paper is to solve an orthogonal problem. We augment simulations such that they exhibit the phenomena of elastic waves and vibrations within the bodies due to impacts, producing movement of objects in contact at a distant locations.

3. Constrained Dynamics

Here we briefly present the constrained multibody dynamics formulation that we use for our rigid simulations. We adopt a symplectic Euler integration scheme and use a time step of size h. Using the velocity-level constrained dynamical equations for an n-body system with m constraint equations, this gives the linear system

$$\begin{bmatrix} \mathbf{M} & -\mathbf{J}^T \\ \mathbf{J} & \frac{1}{h^2}\epsilon\mathbf{I} \end{bmatrix} \begin{bmatrix} \mathbf{v}^+ \\ \lambda^+ \end{bmatrix} = \begin{bmatrix} \mathbf{M}\mathbf{v} + h\mathbf{f} \\ -\frac{\gamma}{h}\phi \end{bmatrix}, \tag{1}$$

with mass matrix $\mathbf{M} \in \mathbb{R}^{6n\times 6n}$, momentum $\mathbf{M}\mathbf{v}$, constraint Jacobian $\mathbf{J} \in \mathbb{R}^{m\times 6n}$, constraint impulses $\lambda \in \mathbb{R}^m$, generalized velocities $\mathbf{v} \in \mathbb{R}^{6n}$, applied forces $\mathbf{f} \in \mathbb{R}^{6n}$, constraint violations $\phi \in \mathbb{R}^m$, and all variables carrying the superscript $\square^+$ are implicit quantities, meaning they are computed at the end of the time step. Note that ϵ provides regularization, and is known as the constraint force mixing parameter (CFM), while γ is the error reduction parameter (ERP) [Smi05]. While these parameters can approximate implicitly integrated elastic contact forces of deformable bodies (e.g., see Galoppo et al. [GOM*06]), we process elastic displacements and vibrations differently for rigid bodies that we equip with distant collision response.

Forming the Schur complement of the upper left block of Equation 1 gives the reduced system

$$\underbrace{\left[\frac{1}{h^2}\epsilon\mathbf{I} + \mathbf{J}\mathbf{M}^{-1}\mathbf{J}^T\right]}_{\mathbf{A}} \lambda^+ = \underbrace{-\frac{\gamma}{h}\phi - \mathbf{J}\mathbf{M}^{-1}(\mathbf{M}\mathbf{v} + h\mathbf{f})}_{\mathbf{b}}, \tag{2}$$

which is a popular formulation for constrained multibody dynamics [ATK17]. Note that the block diagonal form of $\mathbf{M}$ makes it trivial to invert, and since the CFM regularization is diagonal with only positive values, the matrix $\mathbf{A}$ is positive definite and symmetric.

Since our simulations involve contact, we introduce feasibility and complementarity conditions such that

$$\mathbf{A}\lambda^+ - \mathbf{b} = \mathbf{w} = \mathbf{w}_+ - \mathbf{w}_- \tag{3a}$$

$$\begin{cases} \mathbf{0} \le \mathbf{w}_+ \perp \lambda^+ - \lambda_{\text{lo}} \ge \mathbf{0} \\ \mathbf{0} \le \mathbf{w}_- \perp \lambda_{\text{hi}} - \lambda^+ \ge \mathbf{0} \end{cases}, \tag{3b}$$

where λ_{hi} and λ_{lo} are upper and lower bounds on the constraint impulses, respectively. The lower and upper bounds on the constraint impulses $\lambda_{\text{lo}} \le \lambda^+ \le \lambda_{\text{hi}}$ ensure that non-interpenetration constraints λ_{N} only apply forces to separate bodies. Frictional constraints are also bounded according to a box approximation of the Coulomb friction cone and limits are computed as $\lambda_{\text{lo}} = -\mu\lambda_{\text{N}}$ and $\lambda_{\text{hi}} = \mu\lambda_{\text{N}}$, where μ is the static coefficient of friction. We compute the friction bounds based on an initial solution of the non-interpenetration forces λ_{N}, although many iterative solvers [Erl17] allow for more frequent updates of the frictional bounds. Note that we divide the residual vector $\mathbf{w}$ into non-negative complementary components, that is, $\mathbf{0} \le \mathbf{w}_+ \perp \mathbf{w}_- \ge \mathbf{0}$.

For new contacts we can include a Newtonian collision response by modifying $\mathbf{b}$ in Equation 2. Suppose the normal direction contact constraint of the new contact is given by row i of the Jacobian $\mathbf{J}$. We add

$$-\varepsilon\mathbf{J}_{\text{row}i}\mathbf{v} \tag{4}$$

to the i^{th} component of $\mathbf{b}$ where ε is the coefficient of restitution. This ensures that the post-collision relative velocity in the normal direction at the collision is at least as large as ε times the pre-collision relative velocity, and in the opposite direction. When ε is less than 1, the collision response involves energy dissipation in the form of damped elastic vibrations within each colliding object. Conceptually, it is these vibrations that produce our distant collision response.

Once we have the solution of the constraint impulses λ^+, it is then substituted into the first line of Equation 1 to compute the generalized velocities, and we advance the state of the system.

4. Distant Collision Response

We produce two kinds of distant collision responses: one for smaller objects, such as tables, based on activating a modal vibration model and observing displacements at distant contact locations; and one for larger objects, such as terrain or our scaffolding example, which is based on traveling elastic waves that originate at impact locations. We provide details both approaches in the subsections below, beginning with an explanation of how we compute the reduced elastic model.

4.1. Modal Vibrations

To predict the elastic behavior of rigid object we use a reduced linear finite element model. Here we summarize the model reduction technique, and note that the FEMDefo SIGGRAPH course [SB12] provides an excellent detailed overview of many topics related to finite element models and reduced deformation. Let us consider a volume mesh of the rigid object, with n nodes. With damping, small deformations $\mathbf{u} \in \mathbb{R}^{3n}$ of the nodes follow the equation,

$$\mathbf{M}\ddot{\mathbf{u}} + \mathbf{D}\dot{\mathbf{u}} + \mathbf{K}\mathbf{u} = \mathbf{f} \tag{5}$$

where $\mathbf{M}$, $\mathbf{D}$ and $\mathbf{K} \in \mathbb{R}^{3n\times 3n}$ are respectively the mass, damping, and stiffness matrices obtained by applying the finite element method (FEM) to the linearized partial differential equations of elasticity. We use model reduction to project this high-dimensional system onto a low-dimensional subspace to obtain a smaller system with similar properties,

$$\mathbf{u} = \mathbf{U}\mathbf{q} \tag{6}$$

where $\mathbf{U} \in \mathbb{R}^{3n\times m}$ and $\mathbf{q} \in \mathbb{R}^m$ denote the linear *modal basis* matrix and the *modal amplitudes*, respectively (with $m \ll 3n$). The modal basis matrix is an assembly of the *low-frequency* modes obtained by solving the generalized eigenvalue problem of the elastic model, $\mathbf{U} = \{\psi_1, ..., \psi_m\}$. Note that $\mathbf{U}$ is a time-invariant matrix. By substituting Equation 6 into Equation 5 and pre-multiply Equation 5 by $\mathbf{U}^T$, we can then solve for the *amplitudes* $\mathbf{q}$,

$$\mathbf{M}_{\text{q}}\ddot{\mathbf{q}} + \mathbf{D}_{\text{q}}\dot{\mathbf{q}} + \mathbf{K}_{\text{q}}\mathbf{q} = \mathbf{r}, \tag{7}$$

where mass $\mathbf{M}_{\text{q}} = \mathbf{U}^T\mathbf{M}\mathbf{U}$, damping $\mathbf{D}_{\text{q}} = \mathbf{U}^T\mathbf{D}\mathbf{U}$, stiffness $\mathbf{K}_{\text{q}} = \mathbf{U}^T\mathbf{K}\mathbf{U} \in \mathbb{R}^{m\times m}$, and reduced force $\mathbf{r} = \mathbf{U}^T\mathbf{f} \in \mathbb{R}^m$. The matrices $\mathbf{M}_{\text{q}}$ and $\mathbf{K}_{\text{q}}$ are diagonal, and we use Rayleigh damping $\mathbf{D} = \alpha_0\mathbf{M} + \alpha_1\mathbf{K}$ which allows to write the system as m independent ordinary differential equations,

$$\ddot{\mathbf{q}}_i + \left(\alpha_0 + \alpha_1\frac{k_i}{m_i}\right)\dot{\mathbf{q}}_i + \frac{k_i}{m_i}\mathbf{q}_i = \frac{\mathbf{r}_i}{m_i}, \tag{8}$$

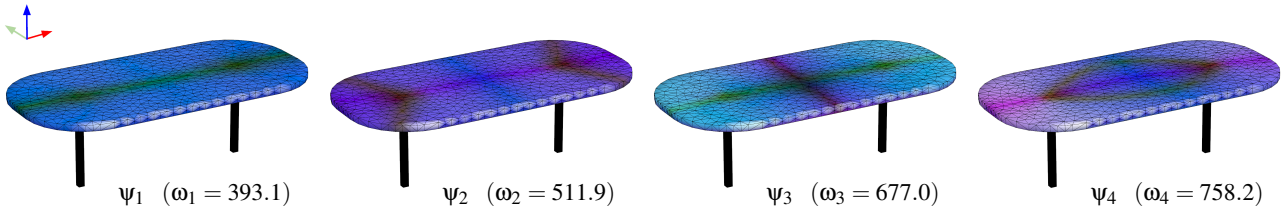

Figure 2: *Four lowest frequency mode shapes of the table model. RGB colors correspond to XYZ absolute displacement magnitudes.*

with m_i and k_i being the i^{th} coefficient of $\text{diag}(\mathbf{M}_\text{q})$ and $\text{diag}(\mathbf{K}_\text{q})$.

In our examples we choose to use 20 modes as we find that this does a reasonable job of capturing the longer lasting low frequency oscillations for the mass, damping, and elasticity parameters we set for our models. For instance, Figure 2 shows the first four modes of the table in Figure 1, which is given parameters for hardwood.

Since we only care about interactions and displacements on the surface of our rigid bodies, we store only the mode information for surface vertices of the tetrahedral mesh in a triangle mesh with matching geometry and surface topology. We then map contact forces and impulses from the rigid body simulation to the surface of this triangle mesh in order to compute the modal displacements due to a collision impulse.

4.2. Displacement Response due to Impact

Our approach simulates collision response at real-time frame rates using an efficient rigid body simulation and it is common to perform collision detection using a geometry that approximates the detailed geometry of the object. We therefore map an impulse due to collision from its location in space to a location on the surface of the triangle mesh of the elastic mechanical model. The process of computing a distant contact response based on collision is summarized in Figure 3.

Given the barycentric coordinates within the model, this impulse of a new contact is mapped to a reduced impulse by

$$\mathbf{r}_c = \mathbf{U}^T \mathbf{H}_c^T \vec{\mathbf{n}}_c \lambda_\text{N} \tag{9}$$

where $\mathbf{U}$ is the reduced basis, $\mathbf{H}_c$ contains the barycentric weights of contact point c, and λ_N is the non-interpenetration impulse from the constraint solve and is in the direction of the contact normal $\vec{\mathbf{n}}_c$.

We apply the reduced impulse vector $\mathbf{r}_c$ to our modal vibration model through forcing. While we could use a soft cosine lobe or Gaussian shape profile, we have already selected a reduced number of modes, and such a softening to avoid activating high frequency modes is unnecessary. Thus, we simply compute the total accumulate reduced impulse from all new contacts that occurred in the rigid body simulation time step, and apply this total as a force at the first time step $\mathbf{r}^{(1)}/T$ where the modal model time step of size T, and use $\mathbf{r}^{(k)} = 0$ for $k > 1$. We compute the response of each mode $\mathbf{q}_j$ due to the forcing function by an IIR digital filter,

$$\mathbf{q}_j^{(k)} = a_{1_j}\mathbf{q}_j^{(k-1)} - a_{2_j}\mathbf{q}_j^{(k-2)} + a_{r_j}\frac{\mathbf{r}^{(k-1)}}{m_j T}, \tag{10}$$

where filter coefficients a_1 and a_2, along with the forcing coefficient a_r, are those specified by James and Pai [JP02]. Recall that T is the time step size for the IIR filter, and $\omega_j = \sqrt{k_j/m_j}$ is the natural undamped frequency of the j^{th} mode. We use an IIR for its simplicity in time stepping the reduced physical system.

Equation 10 is evaluated over a fixed duration that is equal to a single time step h. We step the filter with smaller steps than that of our rigid body simulation. The step size we use is determined by the period of the maximum frequency mode of our reduced model. While we focus only on the low vibration frequencies in our reduced modal model, T can be several orders of magnitude smaller than h. Luckily, the filter response is very efficient to compute. We set the stepping rate of the filter as twice the Nyquist frequency of the maximum modal frequency ω_max:

$$T = \frac{\pi}{2\omega_\text{max}}.$$

4.3. Computing Distant Impulse Responses

We compute an impulse response for each existing contact with the distant collision object. These contacts correspond to mesh locations shown in red in Figure 3, which are nodes in the elastic mechanical model.

Equation 10 computes the nodal displacements at each sub-step k. Since we run the filter at a much higher frame rate than the rigid body simulation, we approximate the response over a time step h and determine the maximum magnitude displacement for each nodal coordinate i corresponding to an existing contact, such that

$$d_{i,\text{max}} = \max_{k=1\ldots h/T} \left| \vec{\mathbf{n}}_i^T \mathbf{U}_i \mathbf{q}^{(k)} \right|, \tag{11}$$

where $\mathbf{U}_i$ is the rows of the modal basis giving the displacement of a distant contact at node i.

The maximum displacement at these distant contacts is used to generate a response by computing a velocity change

$$\Delta v_i = \frac{d_{i,\text{max}}}{h}. \tag{12}$$

This is a velocity change in the normal direction of nodal coordinate i, and for each node affecting contact p we assemble these into a vector of velocity changes $\Delta\mathbf{v}$. Nodal velocities are then mapped back to the contact points p by a simple linear mapping using the barycentric weight matrix for the existing contact $\mathbf{H}_p$:

$$\Delta v_p = \mathbf{H}_p \Delta\mathbf{v}. \tag{13}$$

This quantity can be directly included in Equation 2 by adding it to

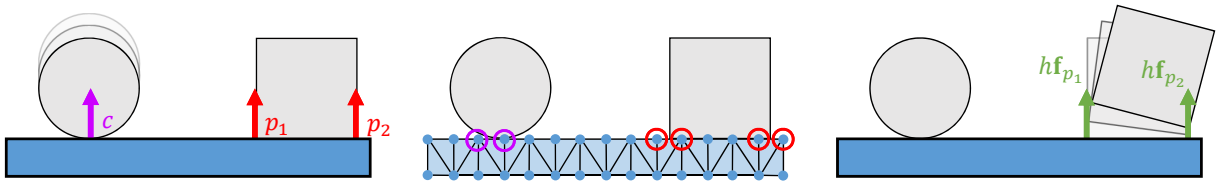

Figure 3: *Left: A sphere collides with a static ground object, which already has a box resting on top. All objects are represented by arbitrary collision proxies, and the collision triggers our distant collision response algorithm. Middle: The contact c (magenta) generated by the impact has its position mapped to points on the surface of the precomputed elastic model using barycentric coordinates. Distant contacts p_1 and p_2 (red) are also identified during this phase. Right: Displacements resulting from the impact vibrations are computed using an IIR filter, which are then converted to impulses applied at distant contact points (green).*

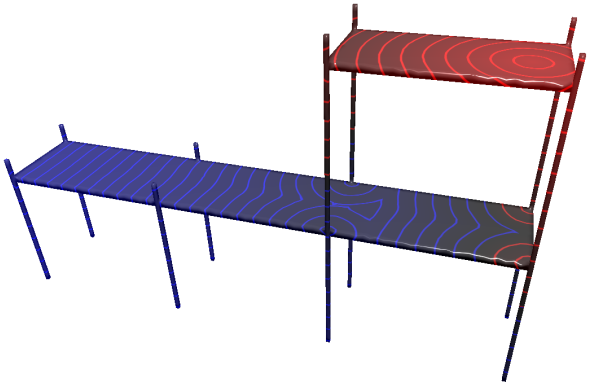

Figure 4: *Geodesic distances computed for a node on the top right hand side of the scaffold mesh.*

the component of **b** corresponding to the normal contact constraint of contact p in the exact same way that we deal with a non-resting contact collision response.

Multiple impacts in the same time step all activate the modal IIR model and the maximum displacement at distant contacts will account for the simultaneous impulses. Furthermore, we can run the IIR continuously, thus small vibrations which have not yet damped can continue to contribute influence distant contact in conjunction with new impacts.

4.4. Distance Collision Response with Spatial Attenuation

In very large objects, such as terrain, an impact does not produce a vibration but instead sends a traveling elastic wave out into the material. An impact produces surface waves, also known as Rayleigh waves, as well as bulk waves beneath the surface. In terrain modeling, it is also recognized that different elastic responses to sheer and compression give waves that travel at different speeds. Since we are mainly interested in the effect of traveling waves observed at distant locations on the surface, we use a geodesic distance between points within an elastic model to compute a response. Note that for flat terrain, this simplifies the distance computation to be a simple Euclidean distance.

The intensity (i.e., energy) of sound waveforms is well-known to follow an inverse proportional square law as a function of distance from the sound source. Terramechanics experiments have also demonstrated that geometric attenuation of vibration in ground terrain follows a similar relationship [CCWT19]. Given a vibration source impacting a terrain surface, the attenuation factor of the waveform amplitude at a distant point is given by

$$s = \exp(-\alpha(r - r_0)) \left(\frac{r}{r_0}\right)^{-\beta}, \tag{14}$$

where r is the distance from the source to the point, r_0 is a minimum distance (i.e., zero attenuation at $r = r_0$), α is a material absorption coefficient, and β is constant that depends on the geometry. The α parameter accounts for energy absorption due to material damping (e.g., Rayleigh damping parameters), The r_0 parameter relates to the discretization of the finite element model because collision at a point produces a brief traction on adjacent elements. The β parameter is similar in spirit to quadratic polynomial light attenuation. However, given that we work with velocities, β is approximately zero for rods structures, 0.5 for thin shells, and 1 for volumes. We discuss later how we take liberties in tuning the parameters of this physically based spatial attenuation model.

To use the attenuation model of Equation 14, we must have an initial displacement amplitude. We precompute the amplitude for a normal unit impulse at each vertex of our mechanical model using the same max displacement procedure described in Section 4.3, except that here we are measuring the displacement of the same vertex that is receiving the impulse. Then, at run time, we simply scale this local displacement amplitude by the attenuation factor in Equation 14 to compute the response at a distant contact. Given an impact c and a vector of displacement due to unit impulse $\hat{\mathbf{q}}$, the local displacement is computed as

$$\Delta x_c = \hat{\mathbf{q}}^T \mathbf{h}_c \lambda_N, \tag{15}$$

where $\mathbf{h}_c$ is a vector containing the barycentric coordinates of the collision location of c and λ_N is the non-interpenetration impulse computed by the constraint solver.

A response at a distance contact p can be produced by modulating the initial amplitude Δx_c according to the to its geodesic distance r_p from the impact point,

$$\Delta v_p = s \frac{\Delta x_c}{h}. \tag{16}$$

Again, we can directly include this in Equation 2 by adding it to the component of **b** corresponding to the normal contact constraint of contact p.

We use a heat-based geodesic computation [CWW13] on the surface mesh to compute the distance r_c between a distant contact and the impact location. While there is only a small cost to compute the distance, we also cache the computation of distances from each existing contact in a hash map. This allows them to be reused if an object only receives a small disturbance, while cached solutions that have not been used in a long time can be periodically removed. Figure 4 shows a visualization of the distances we would cache for an existing contact on the right hand side of the top level of scaffolding for a construction-site.

4.5. Implementation Details

Small magnitude impacts produce effectively no vibration response (e.g., small objects that land gently on a surface need only a small impulse). We reduce computation and do not produce a distant collision response by ignoring impacts in cases where λ_N falls below a set threshold. Furthermore, the IIR filter and spatial attenuation collision response are only computed for new collisions resulting in an impulse greater than the threshold, and so our implementation relies on a callback function that is able to distinguish new collisions from existing collision (e.g., impacts versus resting contacts).

To save time in setting the correct damping parameters, we can choose to completely skip this step and restart the IIR state at zero at the beginning each time step (see Equations 10 and 11). In experiments where we selected good Rayleigh damping parameters, we observe that the vibrations are mostly dissipated after one or two rigid body simulation time steps, and we note that searching for the maximum normal amplitude of the undamped response within a time step h produces effectively the same response.

The exponential decay in the spatial attenuation Equation 14 can have a small effect over the distances that are typical in our scenarios. For easier manual tuning of different scenarios, we set $r_0 = 1$ and replace the exponential with a constant C to simplify the response to $s = Cr^{-\beta}$ in our implementation.

Not all objects in our scenes are equipped with modal vibration models. We have many of the smaller objects in our simulations treated simply as rigid bodies (e.g., plates, cups on the table and tools on the scaffold and roof).

While the convenient way to inject the desired relative velocities at contacts into our rigid body solver is to modify the constraint violation ϕ in Equation 1, the error reduction parameter may not be easy to modify in all rigid body simulation software. In this situation we can directly compute an explicit force (with the drawback that the effect is then injected locally with a local effective mass rather than imposing a desired contact separation velocity on the full solve). That is, we can apply the velocity change at existing contact p as an impulse by multiplying with the effective mass of the contact. This requires computing the effective mass m_{eff} of the contacting body as seen from the non-interpenetration constraint,

$$m_{\text{eff}} = \frac{1}{\mathbf{J}_p \mathbf{M}^{-1} \mathbf{J}_p{}^T} . \tag{17}$$

Finally, the impulse is computed as

$$h\mathbf{f}_p = m_{\text{eff}} \Delta v_p \vec{\mathbf{n}}_p , \tag{18}$$

which is applied to the body with the existing contact p. For a distant collision response with spatial attenuation, the process of computing an impulse from the desired displacement is similar. The response impulse is then computed as

$$h\mathbf{f}_p = s m_{\text{eff}} \frac{\Delta x_c}{h} \vec{\mathbf{n}}_p . \tag{19}$$

5. Results

Our implementation uses the Vortex physics engine [CM 19] for the rigid body simulation. The distant collision response code is implemented in C++ using double precision and the Eigen linear algebra library for matrix multiplications and storage. All simulations were performed on a Windows PC with an Intel Core i9-9980HK (2.4 GHz) CPU and 32 GB of RAM. Table 1 lists compute times for our examples using this hardware.

5.1. Examples

Figures 6-5 show some of the examples we use to demonstrate our distant contact response technique. We summarize some of the simulation parameters for these examples below (see also Table 2), and highlight characteristics of each example. The supplementary video also shows the behavior of each example when simulated using our method.

Dinner is served. A pot (5 kg) is dropped on a table, causing an arrangement of plates (0.5 kg), teacups (0.4 kg), and candlesticks

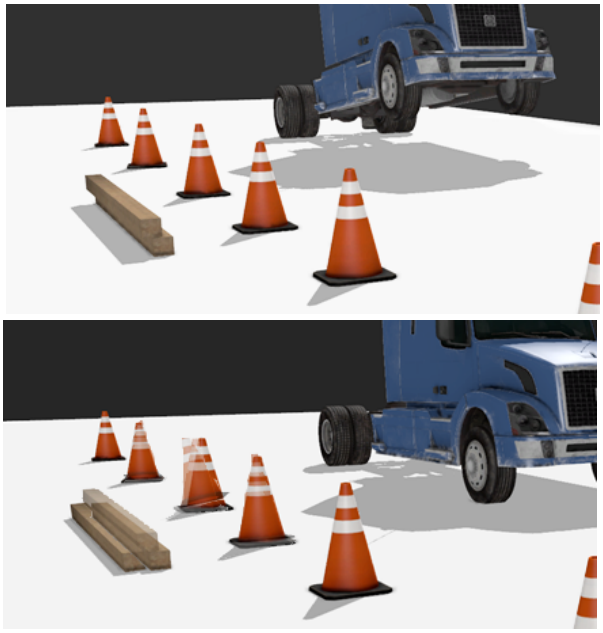

Figure 5: *Nearby traffic cones shake and a stack of lumber topples as a low-rider truck collides with the ground.*

Table 1: *Computation times for the modal vibration response. For each example we name the model with precomputed modes and give the number of vertices and triangles in the surface mesh, the number of modes used, the simulation time step (in seconds), the time step for IIR (in seconds), and the average compute time. Compute times correspond to the IIR solve, the barycentric mapping (back and forward), and the computation of the maximum displacement for all distant contacts.*

Example	Model	# Vertices	# Triangles	# Modes	Time step	Time step (IIR)	# Distant contacts	Compute time
Dinner is served	table	966	1928	20	10^{-2}	4.9×10^{-4}	41	3.8 ms
Wrench on a roof	roof	1002	2000	20	10^{-2}	7.0×10^{-3}	7	0.8 ms
Scaffold	scaffold	5384	10776	20	10^{-2}	3.0×10^{-3}	58	27.5 ms
Low-rider truck	ground	1570	3136	20	10^{-2}	3.1×10^{-4}	40	5.6 ms
Rockfall	cliff	7182	14360	20	10^{-2}	4.0×10^{-3}	24	18.1 ms
Washing machine scene	floor	360	716	20	10^{-2}	1.7×10^{-4}	26	1.1 ms
Washing machine scene	fridge	250	496	20	10^{-2}	8.6×10^{-5}	6	0.2 ms

Table 2: *Parameters used to build the finite element mass and stiffness matrices of each model.*

Model	Young's modulus (GPa)	Poisson ratio	Density (kg/m^3)
table	1.1	0.3	770
cliff	10.0	0.3	500
roof	1.1	0.3	770
scaffold	10.0	0.3	100
ground	10.0	0.3	500
floor	10.0	0.3	540
fridge	1.0	0.3	100

(0.8 kg) to jump as shown in Figure 1. The table is the only object in the simulation with precomputed modes. It is simulated as a static object, and is only used for collision detection and computing the impulse response. We use a density of 700 kg/m^3, Poisson ratio of 0.3, and Young's modulus of 1.1 GPa which is low to account for the fact that our finite element model is solid while a typical table will be constructed from thinner pieces of wood.

Low-rider truck. A semi-truck (10,000 kg) bounces along a ground terrain. The cones (1.0 kg) and wood posts (3.0 kg) shake with each bounce of the truck. One of the wood posts, which is stacked on top of the other, eventually topples and falls to the ground. The ground is only used for collision detection and computing the impulse response. Due to the large scale of this example, we use the approximated impulse response and spatial attenuation described in Section 4.4. An FEM model of a finite slab is used to compute the displacement amplitudes, yet the ground is meant to approximate a very deep and wide terrain. We therefore found that using the average displacement amplitude over surface nodes on the top side of the slab gave more consistent results. This also demonstrates that, for certain models, a plausible response can be computed using only a small number of parameters.

Rockfall. A semi-truck collides with a craggy cliff face, causing rocks from above to come tumbling down, as shown on the left.

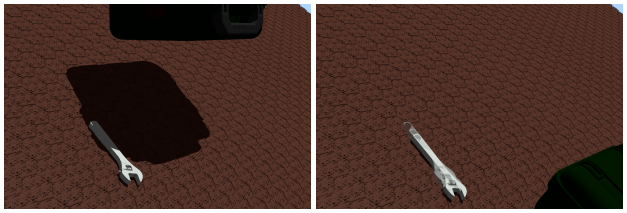

Figure 6: *A heavy toolbox is dropped onto a roof. The responses computed by our method make the wrench slide.*

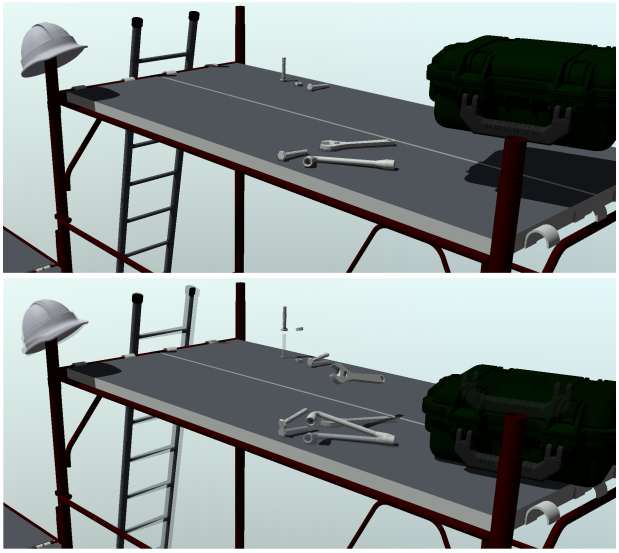

Figure 7: *A heavy toolbox is dropped on a scaffold. The responses computed by our method make the tools jump, and the ladder and the hard hat move.*

We precompute modes of the stone wall mesh, which allows a collision response to be computed for the rocks (50 kg each) that are delicately balanced atop the cliff.

Wrench on a roof. A heavy toolbox (10 kg) is dropped onto a roof as shown in Figure 6. The impacts cause a wrench (0.6 kg), which was resting on the roof, to slightly jump and slide. The roof itself is simulated as a static object, and collision detection with the

Figure 8: *In this simulation, a washing machine is running, making the floor vibrate. Our contact responses make the bottles shake. The vibrations are also propagated to the indoor plant through the fridge.*

toolbox is used to compute the impact response. It can be seen in the supplementary video that the toolbox hits the roof twice, due to a rotational motion. The first impact makes the wrench begin to slide, while the second impact makes it accelerate (visible on the video).

Scaffold. A scaffold holding a variety of tools and protective equipment (0.1 to 0.7 kg) is sent into disarray when a heavy toolbox (10 kg) is dropped from above (see Figure 7). Objects located at the two levels of the scaffold respond differently to the collision (see supplementary video). The scaffold is simulated as a static object.

Washing machine scene. We emulate an unbalanced washing machine by adding artificial impulses to cause it to shake (see Figure 8). Vibrations are propagated through the floor to nearby objects, including a box containing bottles, which are individually simulated as rigid objects, and a fridge with plant. The vibrations are propagated to the plant, causing the leaves to sway. Both the floor and the fridge have precomputed modes. The floor is simulated as a static object and is only used for collision detection and computing the impulse response, while the fridge is a dynamic object. The impulse responses of the floor are impacts on the fridge, which, using the same method, are propagated to the plant laying on top the fridge. This allows to see the leaves sway without necessarily having the fridge moving.

5.2. Ground truth comparison

We compare the result obtained for the Dinner is served example with a reconstruction of this scene simulated using the SOFA [FDD*12] framework, in which the table is a stiff elastic object using the parameters shown in Table 2, and the other objects are rigid (see the supplementary video). The elastic simulation is computed using an implicit integration scheme with a small time step of 10^{-5} to capture the vibrations and high frequency details. The scene, which runs for less than 1 s of simulation time, requires around 30 minutes to compute. The behavior obtained using our IIR filter approach is qualitatively quite similar to the result obtained using the high fidelity simulation. A comparison of the two results can be found in the supplementary video.

Table 3: *Computation times for the spatial attenuation response. We report the first bounce of the Low-rider example separately from the average time of subsequent bounces.*

Example	Compute time
Scaffold	30.6 ms
Low-rider truck (first)	6.9 ms
Low-rider truck (subsequent)	5.2 ms

5.3. Spatial attenuation examples

We demonstrate the spatial attenuation approach for collision response using the Scaffold and Low-rider truck examples. Figure 9 shows the behavior of objects in each of these scenarios as the exponent parameter in Equation 19 is changed (also see these subtle differences between simulations with different parameter values in the supplementary video). We use $\beta = 0.5$, 1.0, and 2.0 in our evaluation and observe that the response becomes more localized as the parameter is increased, which is expected given the role of the term to account for geometric attenuation of an elastic wave.

We experimented with different values for the attenuation scaling coefficient. We found that $C \in [0.4, 1.0]$ produced behavior that was qualitatively similar to the modal collision response, whereas $C \in [1.0, 2.0]$ produced exaggerated, yet plausible, behavior (note the definition of C in Section 4.5).

We also note that it is possible to select plausible parameters with data fitting. Figure 10 shows attenuation samples collected for random locations of impact and distant contacts on the scaffold model. We measure attenuation as a ratio of maximum observed velocities after applying impulses to a high resolution FEM simulation, which uses the elastic parameters specified in Table 2 and Rayleigh parameters $\alpha_0 = 10$ and $\alpha_1 = 10^{-7}$. We note that the best fit attenuation model and hand tuned simplified parameters all correspond to plausible distant collision responses.

The computation of r using the heat-based geodesic solve is done efficiently by caching the result for each heat source, which in our case are the distant contact points since they tend to be coherent across time steps. For example, computing Equation 19 for the first bounce of the Low-rider truck example requires the additional overhead of computing heat geodesic solutions for resting contacts, while in subsequent bounces the computation is largely reduced to a simple hash map lookup. Performance results for computing Equation 19 are summarized in Table 3.

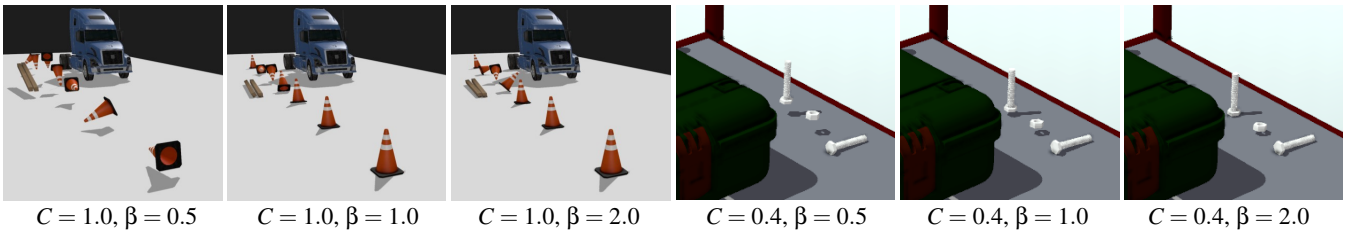

Figure 9: *Spatial attenuation response applied within ground (left) and scaffold (right). Selected frames are shown, highlighting the distant collision response. The attenuation factor C is fixed for each example, while the exponent term* $\beta = 0.5, 1.0, 2.0$ *is varied. A larger value of the exponent creates an increasingly local response to an impact. Note that in the case of the truck example, the response is exaggerated.*

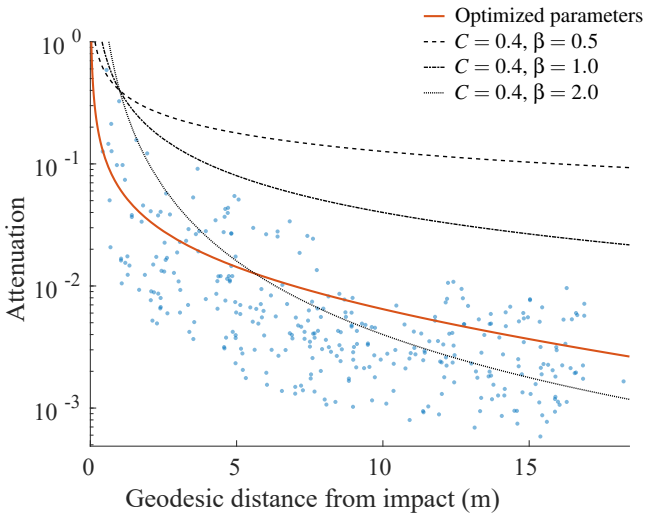

Figure 10: *Scaffold spatial attenuation values measured at random impact and distant contact locations, and curves comparing manually tuned simplified parameters with an optimized fit of* $\alpha = 0.048$, $\beta = 0.8$, *and* $r_0 = 0.033$ *for the parameters of Equation 14.*

5.4. Discussion

The true problem is very messy, and simplifications are necessary to have a solution that can be computed at real-time rates. While our final solution is only a rough approximation of the true behaviour, there is value in using our approach to create a physically inspired elastic response to impacts in rigid body simulations.

One important assumption we make is that collisions and contacts are resolved with impulses computed at the rigid body simulation frame rate. In reality, impacts between elastic objects are resolved with a chain of multiple micro-collisions. These micro-collisions can be baked into the coefficient of restitution [WSJP17], simulated [ZJ11], or in the case of sound synthesis can be specified [vdDKP01]. In our work, we activate vibrations modes with the impulses computed to resolve contacts, and assume that the distant contacts receive an impulse corresponding to the observed specified displacement (as opposed to a set of micro-collisions).

Rayleigh waves and bulk waves through a larger material travel at different speeds, and in larger objects (e.g., terrain) we could need to have response some time steps later in the simulation. But again, we consider all the action to happen within a single time step of the rigid body simulation.

Boundary conditions change the elastic modes, but we pretend that they are not there. This is a large approximation, but we believe it is a necessary simplification to avoid the expensive computations to update our approximation of the elastic wave behaviour with changing boundary conditions. We also note that while we miss out on some subtle and important changes in the elastic response, we still get perhaps a basic physical approximation of the response that provides interesting variation of the coupling of contacts.

We do not have any guarantees for energy conservation. If the coefficient of restitution approaches one we will have perfectly elastic collision response and should not be distributing energy to vibrations in the body and subsequently doing work at distant contacts. That said, because we use small coefficients of restitution our examples (e.g., $\varepsilon = 0.15$) we do not observe anything except energy decay in our examples.

The modal vibrations produced by an impact are not simply in the normal direction and have tangential components too. But in Equation 11, we only search for the largest normal displacement and discard the tangential motion. For frictional surfaces, we may wish to likewise note the lateral displacements during motion in the positive direction and give a lateral kick at distant contacts.

For objects of a sufficiently large size, we can choose to blend our spatially attenuated traveling wave responses described in Section 4.4 with the modal vibration responses describe in Section 4.3. This is an interesting avenue for future work, along with precomputation based methods for estimating good attenuation parameters for Equation 14.

We note that the timings reported in Tables 1 and 3 tend to be dominated by computation of the barycentric coordinates that are used to map collision points in the rigid body simulation to and from the surface mesh storing the elastic model. However, we are certain that optimizing our naive implementation of the barycentric coordinate computation would significantly reduce the computational overhead of our approach.

6. Conclusions

In this paper, we propose two approaches for adding detail to rigid body simulations by taking into account vibrations due to collisions that result in a response at distant contacts at other points on the elastic body. Both approaches are efficient and do not incur the heavy computational cost of simulating stiff elastic body, which makes them suitable for real-time applications.

In the first method, we precompute a generalized eigenvalue decomposition of the elastic model for the distant collision object. Then, we choose a small number of low frequency modes to approximate the response. We qualitatively validated the results obtained using this method against an FEM simulation. For the second method, we compute a spatial attenuation factor based on the geodesic distance from existing contacts to the point where an impact occurred.

We believe that distant collision response has several interesting applications for real-time physics simulations. Our approach adds important secondary dynamics to rigid rigid body simulations. This improves the aesthetics of video games and virtual pre-production applications. However, virtual environment training applications also stand to benefit from our approach since, in the real world, collisions between massive vehicles or machines would result in a significant vibration response. These effects are currently not produced by rigid body simulations.

As part of future work, we would like to validate our approach against further examples using ground truth FEM simulations. Also, since our approach does not consider conservation of energy in the collision response, this is a concern for the plausibility and accuracy of our simulations that we plan to address.

Acknowledgements

We gratefully acknowledge the support of CM Labs Simulations, and the Natural Sciences and Engineering Research Council of Canada (NSERC).

References

[ATK17] ANDREWS S., TEICHMANN M., KRY P. G.: Geometric stiffness for real-time constrained multibody dynamics. *Computer Graphics Forum 36*, 2 (2017), 235–246. 3

[BET13] BENDER J., ERLEBEN K., TRINKLE J. J.: Interactive simulation of rigid body dynamics in computer graphics. *Computer Graphics Forum 33* (2013). 2

[CCWT19] CHEN A., CHENG F., WU D., TANG X.: Ground vibration propagation and attenuation of vibrating compaction. *Journal of Vibroengineering 21*, 5 (2019), 1342–1352. 5

[CM 19] CM LABS SIMULATIONS: Vortex Studio. http://www.cm-labs.com/, 2019. [Online]. 6

[CR98] CHATTERJEE A., RUINA A.: A New Algebraic Rigid-Body Collision Law Based on Impulse Space Considerations. *Journal of Applied Mechanics 65*, 4 (12 1998), 939–951. 2

[CS01] CATALDO E., SAMPAIO R.: A brief review and a new treatment for rigid bodies collision models. *Journal of the Brazilian Society of Mechanical Sciences 23* (00 2001), 63 – 78. 2

[CWW13] CRANE K., WEISCHEDEL C., WARDETZKY M.: Geodesics in heat: A new approach to computing distance based on heat flow. *ACM Trans. Graph. 32*, 5 (Oct. 2013). 6

[EMAK20] ERLEBEN K., MACKLIN M., ANDREWS S., KRY P. G.: The matchstick model for anisotropic friction cones. *Computer Graphics Forum 39*, 1 (2020), 450–461. 2

[Erl07] ERLEBEN K.: Velocity-based shock propagation for multibody dynamics animation. *ACM Trans. Graph. 26*, 2 (2007), 12–es. 2

[Erl17] ERLEBEN K.: Rigid body contact problems using proximal operators. In *Proceedings of the ACM SIGGRAPH / Eurographics Symposium on Computer Animation* (New York, NY, USA, 2017), SCA '17, Association for Computing Machinery. 3

[FDD*12] FAURE F., DURIEZ C., DELINGETTE H., ALLARD J., GILLES B., MARCHESSEAU S., TALBOT H., COURTECUISSE H., BOUSQUET G., PETERLIK I., COTIN S.: SOFA: A Multi-Model Framework for Interactive Physical Simulation. In *Soft Tissue Biomechanical Modeling for Computer Assisted Surgery*, Payan Y., (Ed.), vol. 11 of *Studies in Mechanobiology, Tissue Engineering and Biomaterials*. Springer, 2012, pp. 283–321. 8

[GOM*06] GALOPPO N., OTADUY M. A., MECKLENBURG P., GROSS M., LIN M. C.: Fast simulation of deformable models in contact using dynamic deformation textures. In *Proceedings of the 2006 ACM SIGGRAPH/Eurographics Symposium on Computer Animation* (2006), SCA '06, p. 73–82. 2, 3

[JP02] JAMES D. L., PAI D. K.: DyRT: Dynamic response textures for real time deformation simulation with graphics hardware. In *Proceedings of the 29th Annual Conference on Computer Graphics and Interactive Techniques* (New York, NY, USA, 2002), SIGGRAPH '02, Association for Computing Machinery, p. 582–585. 4

[KCMF12] KIM T.-Y., CHENTANEZ N., MÜLLER-FISCHER M.: Long range attachments - a method to simulate inextensible clothing in computer games. In *Proceedings of the ACM SIGGRAPH/Eurographics Symposium on Computer Animation* (2012), pp. 305–310. 2

[MCMJ17] MÜLLER M., CHENTANEZ N., MACKLIN M., JESCHKE S.: Long range constraints for rigid body simulations. In *Proceedings of the ACM SIGGRAPH / Eurographics Symposium on Computer Animation* (2017), SCA '17, pp. 14:1–14:10. 2

[OSG02] O'BRIEN J. F., SHEN C., GATCHALIAN C. M.: Synthesizing sounds from rigid-body simulations. In *Proceedings of the 2002 ACM SIGGRAPH/Eurographics Symposium on Computer Animation* (2002), SCA '02, p. 175–181. 2

[PDJ*01] PAI D. K., DOEL K. V. D., JAMES D. L., LANG J., LLOYD J. E., RICHMOND J. L., YAU S. H.: Scanning physical interaction behavior of 3d objects. In *Proceedings of the 28th Annual Conference on Computer Graphics and Interactive Techniques* (2001), SIGGRAPH '01, p. 87–96. 2

[PPG04] PAULY M., PAI D. K., GUIBAS L. J.: Quasi-rigid objects in contact. In *Proceedings of the 2004 ACM SIGGRAPH/Eurographics Symposium on Computer Animation* (2004), SCA '04, p. 109–119. 2

[SB12] SIFAKIS E., BARBIC J.: FEM simulation of 3D deformable solids: A practitioner's guide to theory, discretization and model reduction. In *ACM SIGGRAPH 2012 Courses* (2012), SIGGRAPH '12. 3

[SKV*12] SMITH B., KAUFMAN D. M., VOUGA E., TAMSTORF R., GRINSPUN E.: Reflections on simultaneous impact. *ACM Transactions on Graphics (Proceedings of SIGGRAPH 2012) 31*, 4 (2012), 106:1–106:12. 2

[Smi05] SMITH R.: Open dynamics engine. https://ode.org/ode-latest-userguide.html, 2005. 3

[vdDKP01] VAN DEN DOEL K., KRY P. G., PAI D. K.: FoleyAutomatic: Physically-based sound effects for interactive simulation and animation. In *Proceedings of the 28th Annual Conference on Computer Graphics and Interactive Techniques* (2001), SIGGRAPH '01, p. 537–544. 2, 9

[WSJP17] WANG J.-H., SETALURI R., JAMES D. L., PAI D. K.: Bounce maps: An improved restitution model for real-time rigid-body impact. *ACM Trans. Graph. 36*, 4 (July 2017). 2, 9

[ZJ11] ZHENG C., JAMES D. L.: Toward high-quality modal contact sound. In *ACM SIGGRAPH 2011 Papers* (New York, NY, USA, 2011), SIGGRAPH '11, Association for Computing Machinery. 2, 9